

Accepted Manuscript

Title: Simultaneous catalytic oxidation of carbon monoxide, hydrocarbons and soot with Ce-Zr-Nd mixed oxides in simulated Diesel exhaust conditions

Author: Leandro P. dos Santos Xavier Verónica Rico-Pérez
Ana M. Hernández-Giménez Dolores Lozano-Castelló
Agustín Bueno-López



PII: S0926-3373(14)00411-1
DOI: <http://dx.doi.org/doi:10.1016/j.apcatb.2014.07.013>
Reference: APCATB 13444

To appear in: *Applied Catalysis B: Environmental*

Received date: 21-5-2014
Revised date: 3-7-2014
Accepted date: 5-7-2014

Please cite this article as: L.P.S. Xavier, V. Rico-Pérez, A.M. Hernández-Giménez, D. Lozano-Castelló, A. Bueno-López, Simultaneous catalytic oxidation of carbon monoxide, hydrocarbons and soot with Ce-Zr-Nd mixed oxides in simulated Diesel exhaust conditions, *Applied Catalysis B, Environmental* (2014), <http://dx.doi.org/10.1016/j.apcatb.2014.07.013>

This is a PDF file of an unedited manuscript that has been accepted for publication. As a service to our customers we are providing this early version of the manuscript. The manuscript will undergo copyediting, typesetting, and review of the resulting proof before it is published in its final form. Please note that during the production process errors may be discovered which could affect the content, and all legal disclaimers that apply to the journal pertain.

1 **Simultaneous catalytic oxidation of carbon**
2 **monoxide, hydrocarbons and soot with Ce-Zr-Nd**
3 **mixed oxides in simulated Diesel exhaust**
4 **conditions.**

5 Leandro P. dos Santos Xavier, Verónica Rico-Pérez, Ana M. Hernández-
6 Giménez, Dolores Lozano-Castelló, Agustín Bueno-López*.

7
8 Department of Inorganic Chemistry. University of Alicante, Ap.99, E-03080
9 Alicante (Spain).

10 *Corresponding author: email: agus@ua.es; Tel. +34 600948665; Fax. +34 965903454
11

12 **Abstract**

13 $\text{Ce}_{0.73-x}\text{Zr}_{0.27}\text{Nd}_x\text{O}_2$ mixed oxides ($x \leq 0.3$) were prepared, characterized
14 by XRD, Raman spectroscopy, N_2 adsorption isotherms and H_2 -TPR, and
15 tested for simultaneous CO, propylene, benzene and soot oxidation in a gas
16 mixture containing O_2 , NO_x , H_2O , CO_2 , CO, propylene (model aliphatic
17 hydrocarbon) and benzene (model aromatic hydrocarbon) that simulates a
18 Diesel exhaust. Ce-Zr mixed oxide doping with a low atomic fraction of
19 neodymium ($0.01 \leq x \leq 0.09$) promotes the creation of oxygen vacancies, has a
20 minor effect in the BET specific surface areas of the oxides, increases the
21 surface ceria reducibility and has a positive effect in the catalytic activity. On the
22 contrary, higher neodymium atomic fractions ($x = 0.2$ and 0.3) promote
23 sintering, with a drastic decrease of the BET specific surface area, surface
24 reducibility and catalytic activity. The $\text{Ce}_{0.73-x}\text{Zr}_{0.27}\text{Nd}_x\text{O}_2$ catalysts with $x \leq 0.09$
25 are able to accelerate simultaneously soot, propylene and benzene combustion,
26 and as a general trend, the catalytic behavior of $\text{Ce}_{0.73}\text{Zr}_{0.27}\text{O}_2$ is improved by
27 low atomic fraction neodymium doping ($0.01 \leq x \leq 0.09$). These $\text{Ce}_{0.73-}$
28 $x\text{Zr}_{0.27}\text{Nd}_x\text{O}_2$ mixed oxides with $0.01 \leq x \leq 0.09$ are also able to accelerate CO
29 oxidation in a certain extent, but there is a net production of CO during soot
30 combustion because the oxidation capacity of these oxides is not high enough
31 to oxidize all CO released as soot combustion product.

32
33
34 **Keywords:** Diesel soot; carbon monoxide; hydrocarbons; ceria-zirconia
35 catalyst; neodymium-ceria catalyst.

36

37 **1.- Introduction.**

38 Cerium-based oxides are part of the active phases used in Three Way
39 Catalysts (TWC) for gas pollution control in gasoline vehicles [1-4]. Cerium
40 oxides improve noble metals dispersion and stabilization, store and release
41 oxygen buffering the fluctuations of the O₂ concentration in the gas mixture and
42 catalyze (together with noble metals) some reactions like CO and hydrocarbons
43 oxidation.

44 Cerium oxide-based catalysts have been also proposed for soot
45 combustion in Diesel vehicles, where the gas exhaust is highly oxidizing [5-9].
46 Diesel engines also emit CO and hydrocarbons, but in much lower
47 concentration than gasoline engines [10-13]. Usually, a platinum-containing
48 Diesel Oxidation Catalyst (DOC) is used in Diesel vehicles for simultaneous
49 CO, hydrocarbons and NO oxidation. The NO₂ produced, which is much more
50 oxidizing than NO and O₂, starts the combustion of soot collected downstream
51 in a Diesel Particulate Filter (DPF).

52 Noble metal-free catalysts are being investigated for soot combustion in
53 Diesel exhausts in order to lower the cost of the after-treatment devices. Ceria-
54 based oxides are promising candidates, and the role of O₂ and NO_x in the
55 ceria-catalyzed combustion of soot is well understood. One of the ceria-
56 catalyzed soot-combustion mechanisms consists of the oxidation of NO to NO₂
57 (as described for platinum-containing DOC), and other consists of the
58 production of active oxygen by oxygen exchange between the ceria-based
59 catalyst and the oxygen-containing gas molecules, mainly O₂. Depending on the

60 ceria catalyst features and on the reaction conditions (temperature, gas
61 composition, etc.) either both mechanisms progress synergically together or
62 one of them prevails.

63 Platinum catalysts are much more active for NO oxidation to NO₂ than
64 ceria catalysts, but the latter are able to approach the activity of platinum for
65 soot combustion if the active oxygen mechanism gets involved. The main
66 handicap of the active oxygen mechanism is that the contact between soot and
67 ceria catalyst particles must allow the active oxygen species to be transferred
68 from catalyst to soot, otherwise they recombine to each other and yield O₂ [14].
69 Therefore, ceria catalysts must be impregnated into the DPF instead of being
70 loaded in a DOC located upstream the DPF, as usually done with platinum.

71 The substitution of the Pt-DOC + DPF soot removal device by a Ceria-
72 DPF configuration seems promising, but it must be analyzed whether ceria-
73 catalysts are able to remove simultaneously soot, hydrocarbons and CO, as
74 platinum catalyst does, or if further improvements are required.

75 We have recently analyzed the effect of H₂O, CO₂ and SO₂ in the
76 catalytic activity for soot combustion of Ce_{0.73}Zr_{0.27}O₂ and Ce_{0.64}Zr_{0.27}Nd_{0.09}O₂ in
77 simulated Diesel exhaust conditions, concluding that all these three gases lower
78 the activity of both catalysts and that the inhibiting effect follows the trend SO₂
79 >>> H₂O > CO₂ [15]. The poisoning effect of SO₂ was already reported by other
80 authors [16-19], but less attention was paid in the literature to the effect of H₂O
81 and CO₂. In situ DRIFTS experiments showed that CO₂, H₂O and SO₂ compete
82 with NO_x for the adsorption sites on the catalysts' surface [15]. CO₂ and H₂O
83 partially hinder the catalytic oxidation of NO to NO₂ while SO₂ chemisorption

84 inhibits almost all the activity due to sulfate formation. The catalytic activity for
85 soot combustion of $\text{Ce}_{0.64}\text{Zr}_{0.27}\text{Nd}_{0.09}\text{O}_2$ was equal or higher to that of
86 $\text{Ce}_{0.73}\text{Zr}_{0.27}\text{O}_2$ in the presence of NO_x , O_2 , H_2O and/or CO_2 , because Nd^{3+}
87 doping promotes the participation of the active oxygen mechanism, which
88 seems to resist the presence of H_2O and CO_2 better than the NO_2 -assisted
89 soot combustion mechanism [15]. For this reason, the $\text{Ce}_{0.64}\text{Zr}_{0.27}\text{Nd}_{0.09}\text{O}_2$
90 mixed oxide was identified as a potential catalyst with practical relevance for
91 Diesel vehicles running with sulfur-free fuel, since it maintained significant
92 activity for soot combustion even in the presence of H_2O and CO_2 .

93 As far as we know, the simultaneous ceria-catalyzed combustion of soot,
94 CO, and hydrocarbons has not been studied and reported in the literature, and
95 this is one of the goals of the current study. In addition, the positive effect of
96 Nd^{3+} doping in the catalytic activity of the Ce-Zr mixed oxide for soot combustion,
97 which was first reported in [20], has led us to focus the current study on ternary
98 Ce-Zr-Nd mixed oxides. A series of $\text{Ce}_{0.73-x}\text{Zr}_{0.27}\text{Nd}_x\text{O}_2$ mixed oxides were
99 prepared with different neodymium content, and were characterized and tested
100 for the simultaneous oxidation of CO and hydrocarbons, both in the absence
101 and presence of soot. A complex gas mixture that mimics a Diesel engine
102 exhaust containing NO_x , O_2 , H_2O , CO_2 , CO, propylene and benzene was used.
103 Propylene and benzene were selected as model aliphatic and aromatic
104 hydrocarbons, respectively.

105 **2.- Experimental details.**

106 *2.1. Catalysts preparation.*

107 Six $\text{Ce}_{0.73-x}\text{Zr}_{0.27}\text{Nd}_x\text{O}_2$ mixed oxides were prepared, with $x = 0, 0.01,$
108 $0.05, 0.09, 0.2$ and 0.3 . Formally, the stoichiometric coefficient of oxygen in the
109 neodymium-containing catalysts should be lower than 2, since the tetravalent
110 cation " Ce^{4+} " is replaced by a trivalent one (Nd^{3+}). However, the subscript 2 has
111 been maintained in the nomenclature for the sake of simplicity.

112 The required amounts of $\text{Ce}(\text{NO}_3)_3 \cdot 6\text{H}_2\text{O}$ (Sigma Aldrich, 99%),
113 $\text{Nd}(\text{NO}_3)_3 \cdot 6\text{H}_2\text{O}$ (Aldrich, 99.9%) and/or $\text{ZrO}(\text{NO}_3)_2 \cdot x\text{H}_2\text{O}$ (Fluka, $x \approx 6$) were
114 dissolved in water and an ammonia solution was dropped to keep the pH at
115 about 9, leading to the precipitation of the cations. After filtering, the precipitates
116 were firstly dried at $110\text{ }^\circ\text{C}$ in air overnight and then calcined in air at $800\text{ }^\circ\text{C}$ for
117 90 min to ensure thermal stability and practical meaning.

118 The synthesis method and the amount of zirconium on the mixed oxides
119 were selected based on our previous studies on soot combustion, where
120 catalysts with different Ce-Zr ratios were prepared by different methods [21, 22].

121 *2.2. Catalysts characterization.*

122 X-ray diffractograms of the catalysts were recorded in a Rigaku Miniflex II
123 diffractometer, using CuK_α radiation ($\lambda = 0.15418\text{ nm}$). The diffractograms were
124 recorded between 10 and 80° (2θ) with a step of 0.025° .

125 Raman spectra were recorded in a Bruker RFS 100/S Fourier Transform
126 Raman Spectrometer with a variable power Nd-YAg laser source (1064 nm).
127 The laser beam was focused on the sample in a 180° backscattering
128 configuration and 128 scans at 100 mW laser power were recorded.

129 The BET specific surface area of the oxides was determined by physical
130 adsorption of N₂ at -196 °C in an automatic volumetric system (Autosorb-6,
131 Quantachrome). The samples were outgassed at 150 °C for 4 hours before the
132 N₂ adsorption measurements.

133 Temperature programmed reduction (H₂-TPR) experiments were carried
134 out with 15 mg of fresh mixed oxide, which were pre-treated *in situ* at 500 °C for
135 1 hour in a 35 mL/min flow of 5 vol.% O₂ in He. Once cold, the flow gas was
136 switched to 35 mL/min of 5 vol.% H₂ in Ar and the temperature was increased at
137 10 °C/min up to 1050 °C.

138 2.3. Catalytic tests.

139 Catalytic tests were performed at atmospheric pressure in a cylindrical
140 reactor coupled simultaneously to a HP 6890 gas chromatograph equipped with
141 a TCD and two columns (Porapak Q, for CO₂ and Molecular Sieve 13X, for O₂,
142 N₂ and CO) and a Pfeiffer Vacuum mass spectrometer (model OmniStar) to
143 monitor NO, propylene, NO₂ and benzene concentrations following the m/z =
144 30, 39, 46 and 78 signals, respectively. The total flow rate was 100 ml/min
145 (GHSV = 42000 h⁻¹) and the gas composition was 300 ppm CO / 120 ppm
146 propylene / 3% CO₂/ 180 ppm benzene / 1000 ppm NO_x (~ 0 ppm NO₂) / 5%O₂
147 / 2%H₂O and He as balance gas. Gas flow controllers were used to feed the
148 required amount of each individual gas, and the O₂ flow was bubbled in water at
149 72 °C before mixing with the remaining flows to add steam into the gas mixture.
150 This complex composition simulates a real Diesel engine exhaust and allows
151 evaluating the simultaneous catalytic oxidation of CO, propylene, benzene and
152 soot in quite realistic conditions.

153 Catalytic tests were performed with and without soot. Experiments
154 performed without soot consisted of the simultaneous CO, propylene and
155 benzene catalytic oxidation studied at selected temperatures from room
156 temperature up to 550 °C. 100 mg of each mixed oxide catalyst were used for
157 these experiments, which were diluted with 300 mg of SiC to avoid pressure
158 drop and favor heat transfer. The experiments were extended until steady-state
159 at each temperature, typically for 30 minutes.

160 Experiments were also performed with 100 mg of catalyst mixed with 25
161 mg of soot and 300 mg of SiC. Soot and catalyst were mixed with a spatula in
162 the so-called loose contact conditions to simulate the contact in a real DPF filter
163 [23]. The model soot used was a carbon black supplied by Evonik–Degussa
164 GmbH (Printex U). The soot-catalyst-SiC mixture was heated at 530 °C in 13
165 mL/min He. Then, the inert gas was replaced by the reactive gas mixture and
166 the gas composition was monitored as a function of time.

167 Propylene and benzene conversions were determined following the m/z
168 39 and 78 signals, respectively, by mass spectrometry and CO conversions
169 were determined from gas chromatography measurements. The conversions of
170 CO, propylene and benzene were calculated as follows:

$$171 \quad \text{Conversion (\%)} = 100 \cdot ([\text{pollutant}]_{\text{in}} - [\text{pollutant}]_{\text{out}}) / [\text{pollutant}]_{\text{in}}$$

172 where $[\text{pollutant}]_{\text{in}}$ and $[\text{pollutant}]_{\text{out}}$ are the inlet and outlet concentrations,
173 respectively, of each gas pollutant (CO, propylene and benzene).

174 Soot conversion was determined from CO₂ and CO evolved (both
175 followed by gas chromatography) after subtracting the stoichiometric amounts

176 of CO₂ corresponding to the propylene, benzene and CO conversions assuming
177 oxidation of these gases to CO₂ and H₂O.

178

179 **3.- Results and discussion.**

180 *3.1. Catalysts characterization.*

181 Figure 1 shows the X-ray diffractograms of the Ce_{0.73-x}Zr_{0.27}Nd_xO₂
182 catalysts. The main peaks observed in this figure correspond to the typical cubic
183 structure of ceria. A shoulder is also distinguished in all diffractograms at high
184 angles of the (111) cubic peak, which evidences the formation of a tetragonal
185 segregated phase. The cations sublattice is similar in the cubic and tetragonal
186 structures, corresponding to a face-centered cubic (fcc) framework with cations
187 placed in the corners and faces center of a cubic unit cell. The difference
188 between the cubic and tetragonal frameworks is the position of the oxygen
189 anions. Oxygen anions are placed in the octahedral positions in the cubic
190 structure while they are out these positions (four above and four below the
191 equilibrium positions) in the tetragonal structure [24-27]. Tetragonalization of
192 the cubic structure of pure ceria typically occurs upon partial substitution of the
193 Ce⁴⁺ cations (0.097 nm) by smaller Zr⁴⁺ cations (0.084 nm), because the
194 oxygen anions are displaced from the octahedral position to relax the tensions
195 created by different size cations. The segregation of a cerium-rich cubic
196 structure and a zirconium-rich tetragonal structure was already observed for
197 Ce_{0.73}Zr_{0.27}O₂ and Ce_{0.64}Zr_{0.27}Nd_{0.09}O₂ oxides [20], and this conclusion is now
198 extended to a wider range of neodymium atomic fractions.

199 The XRD peaks positions, intensity and broadening strongly depends on
200 the neodymium atomic fraction (see inset in Figure 1), because the introduction
201 of large trivalent Nd^{3+} cations (0.112 nm) distorts the lattices. The crystal sizes
202 have not been estimated from XRD because the presence of the segregated
203 tetragonal zirconium-rich phase hinders the proper estimation of the cubic
204 peaks broadening. It is also difficult to quantify the amount of dopants actually
205 loaded into the ceria lattice for ternary Ce-Zr-Nd mixed oxides, because the cell
206 expansion produced by Nd^{3+} doping faces the cell contraction produced by
207 Zr^{4+} doping. However, some information can be obtained from the cell
208 parameters determined from the (111) peak position, which can be properly
209 determined for all oxides in spite of the tetragonal peak shoulder. The
210 experimentally measured cell parameters are plotted in Figure 2 together with
211 the theoretical values estimated for pure Ce-Zr-Nd solid solutions using the
212 Kim's equation [28, 29]:

$$213 \quad \text{Cell parameter (nm)} = 0.5411 - 0.000286 \cdot m_{\text{Zr}} + 0.00018 \cdot m_{\text{Nd}}$$

214 where m_{Zr} and m_{Nd} are the atomic % of zirconium and neodymium in the Ce-Zr-
215 Nd solid solution, respectively. This empirical equation is based on the Vegard's
216 rule, which predicts a linear relationship between the lattice parameter and the
217 concentration of dopants in a solid solution.

218 The experimental cell parameters of all samples are well above the
219 theoretical trend predicted for a pure solid solution, in agreement with the
220 segregation of part of the zirconium in a tetragonal phase. For $\text{Ce}_{0.73-}$
221 $\text{xZr}_{0.27}\text{Nd}_x\text{O}_2$ mixed oxides with $x \leq 0.09$, the slope of the linear trend followed by
222 the experimental values with regard to the neodymium concentration is quite

223 similar to that predicted by the Kim's equation, suggesting that the insertion of
224 neodymium cations into the cubic lattice of ceria is quite good and better to that
225 of zirconium. This slope decreases for higher neodymium concentrations, which
226 suggests that Nd^{3+} loading into the parent ceria lattice becomes more difficult
227 for 0.2 and 0.3 neodymium atomic fractions.

228 The better insertion of neodymium cations into the ceria lattice in
229 comparison with those of zirconium can be explained taking into account the
230 charge of the cations precursors used for the preparation of the mixed oxides,
231 being +3 for cerium and neodymium while +4 for zirconium. The coprecipitation
232 of cations upon ammonia adding is much more homogeneous for cations with
233 the same charge and similar size (0.114 nm for Ce^{3+} and 0.112 nm for Nd^{3+}),
234 because their acid strength is similar, than for cations of different charge and
235 size. That is why, in the current study, cerium and neodymium formed better
236 solid solutions than cerium and zirconium. It must be taken into account that
237 cerium precursors with both +3 and +4 charges exist, while not for zirconium
238 and neodymium which are only available in the +4 and +3 oxidation states,
239 respectively. Our choice for the current study was to use a Ce^{3+} precursor
240 because the study is focused on the effect of neodymium loading, but in a
241 previous article the effect of the cerium precursor in the features of binary Ce-Zr
242 oxides was discussed in detail [30]. It is known that much better insertion of Zr^{4+}
243 into the ceria framework would be obtained with the selection of a Ce^{4+}
244 precursor, but this would be hindered Nd^{3+} doping.

245 Raman spectra included in Figure 3 also provided information about the
246 structure of the oxides, and supported some conclusions of the XRD analysis.

247 All spectra show a Raman band centered at $460\text{--}465.8\text{ cm}^{-1}$, which is assigned
248 to the F_{2g} mode of the fluorite-type cubic structure of cerium oxides [31, 32]. The
249 presence of low-intensity bands in the range $120\text{--}300\text{ cm}^{-1}$ has been related to
250 the tetragonal shift of the oxygen anions from the ideal octahedral positions that
251 occupy in the fluorite cubic structure [33, 34], which typically occurs upon
252 zirconium insertion into the CeO_2 lattice. The displacement of the F_{2g} band
253 position towards low Raman shifts by increasing the neodymium atomic fraction
254 (see Figure 3b) is an evidence of the introduction of large Nd^{3+} cations into the
255 parent cubic structure of ceria. The creation of oxygen vacancies is related to
256 the shoulder at 620 cm^{-1} [35], and the intensity of this shoulder suggests that
257 the number of vacancies increases significantly for low neodymium atomic
258 fractions ($x \leq 0.09$) but it is not so relevant for higher neodymium content ($x =$
259 0.2 and 0.3). This is consistent with the cell parameter trend determined by
260 XRD (see Figure 2), which suggested that the neodymium insertion becomes
261 worse for mixed oxides with 0.2 and 0.3 neodymium atomic fractions.

262 The BET specific surface areas also showed important differences
263 among $\text{Ce}_{0.73-x}\text{Zr}_{0.27}\text{Nd}_x\text{O}_2$ mixed oxides. The values plotted in Figure 4 show
264 that the BET specific surface areas ranged from 0 to $31\text{ m}^2/\text{g}$. These low values
265 were expected considering that the oxides were sintered at $800\text{ }^\circ\text{C}$ to provide
266 practical meaning to the study. The BET surface area of the neodymium-free
267 Ce-Zr mixed oxide ($26\text{ m}^2/\text{g}$) is in line with typical values previously obtained for
268 similar materials with the same thermal history [20, 21], and slightly higher
269 areas were obtained for $\text{Ce}_{0.73-x}\text{Zr}_{0.27}\text{Nd}_x\text{O}_2$ oxides with $0.01 \leq x \leq 0.09$.
270 However, higher neodymium atomic fractions lead to an important sintering of
271 the mixed oxides with a drastic decrease of the BET surface area down to 8 and

272 0 m²/g for x = 0.2 and 0.3, respectively. The existence of an optimum dopant
273 loading has been already reported for some other mixed oxides. Zhang et al.
274 [36, 37] studied La³⁺-doped TiO₂ oxides and reported that the optimum
275 lanthanum atomic fraction was 1% in order to avoid the phase transformation of
276 titania. This amount of lanthanum was estimated to correspond to a monolayer
277 of surface cations, and further increase of the dopant concentration above the
278 monolayer coverage induced the segregation of lanthanum oxide and titanium
279 oxide. This argument could also be applied to our Ce_{0.73-x}Zr_{0.27}Nd_xO₂ mixed
280 oxides, that is, low neodymium atomic fractions ($x \leq 0.09$) seem to slightly
281 stabilize the mixed oxide, while higher neodymium contents have the opposite
282 effect, in spite of evidences of segregated neodymium phases were neither
283 obtained by XRD nor by Raman spectroscopy.

284 Characterization of the mixed oxides was also carried out by
285 Temperature Programed Reduction with H₂, and the obtained profiles were
286 drawn in Figure 5. Note that the only reducible cations in the Ce_{0.73-x}Zr_{0.27}Nd_xO₂
287 mixed oxides are Ce⁴⁺, while both Zr⁴⁺ and Nd³⁺, which cannot be reduced in
288 the experimental conditions of the H₂-TPR experiments, modify the redox
289 behavior of the Ce⁴⁺/Ce³⁺ couple.

290 Most H₂-TPR profiles consist of a mild-temperature peak around 550 °C,
291 which is attributed to surface reduction of the mixed oxides, and a high-
292 temperature peak assigned to bulk reduction. The formation of two well-defined
293 reduction peaks in most of the mixed oxides studied occurs because there is an
294 energetic restriction for the bulk oxygen to move until the particles surface, and
295 high temperature is required to promote such oxygen mobility.

296 The surface and bulk reduction-peak temperatures are plotted in Figure 6
297 versus the neodymium atomic fraction. The neodymium loading affected both
298 the surface and bulk reduction. The bulk reduction peak shifted towards lower
299 temperature with the neodymium content increase (see Figure 6), and the
300 surface and bulk reduction peaks even merge for the highest neodymium-
301 content mixed oxides (see Figure 5). This occurs because the introduction of
302 large trivalent Nd^{3+} cations into the parent ceria-zirconia framework improves
303 the mobility of oxygen into the lattice, and only 0.01 neodymium atomic fraction
304 is enough to shift significantly the bulk reduction peak. The effect of neodymium
305 on surface reduction was the opposite, and the surface reduction-peak
306 temperature was delayed towards higher temperatures as the neodymium
307 atomic fraction was increased. This delay was small for $\text{Ce}_{0.73-x}\text{Zr}_{0.27}\text{Nd}_x\text{O}_2$
308 mixed oxides with $x \leq 0.09$, but became much more relevant for $x = 0.2$ and 0.3 ,
309 which is consistent with the very low surface area of these two mixed oxides (8
310 and $0 \text{ m}^2/\text{g}$). However, the area under the surface reduction peak (see Figure 5)
311 increased for $\text{Ce}_{0.72}\text{Zr}_{0.27}\text{Nd}_{0.01}\text{O}_2$ and $\text{Ce}_{0.68}\text{Zr}_{0.27}\text{Nd}_{0.05}\text{O}_2$ with respect to
312 $\text{Ce}_{0.73}\text{Zr}_{0.27}\text{O}_2$, that is, few neodymium increased the amount of surface Ce^{4+}
313 reduced.

314 As a summary, the characterization results have shown that the $\text{Ce}_{0.73-}$
315 $x\text{Zr}_{0.27}\text{Nd}_x\text{O}_2$ mixed oxides prepared consist of two segregated ceria-rich and
316 zirconium rich phases with proper neodymium doping for $x \leq 0.09$. This is a
317 consequence of the preparation method used, where Ce^{3+} , Nd^{3+} and Zr^{4+}
318 cations were precipitated. Doping the Ce-Zr mixed oxides with low atomic
319 fractions of neodymium promoted the creation of oxygen vacancies, had a
320 minor effect on the BET specific surface area of the oxides, increased the

321 amount of surface Ce^{4+} reduced and, as it will be discussed in the coming
322 section, had a positive effect on the catalytic activity. On the contrary, higher
323 neodymium atomic fractions ($x = 0.2$ and 0.3) had a negative effect on the
324 mixed oxides features because promote sintering, with a drastic decrease of the
325 BET specific surface area and of the surface reducibility. These worst features
326 of $\text{Ce}_{0.53}\text{Zr}_{0.27}\text{Nd}_{0.2}\text{O}_2$ and $\text{Ce}_{0.43}\text{Zr}_{0.27}\text{Nd}_{0.3}\text{O}_2$ are also evidenced in the catalytic
327 behavior in the next section.

328 3.2. Catalytic tests.

329 Catalytic tests were performed with the $\text{Ce}_{0.73-x}\text{Zr}_{0.27}\text{Nd}_x\text{O}_2$ oxides in the
330 absence and presence of soot under a complex gas mixture with O_2 , NO_x , H_2O ,
331 CO_2 , CO , propylene (model aliphatic hydrocarbon) and benzene (model
332 aromatic hydrocarbon). The consumption of NO_x was negligible in all cases,
333 and the discussion is focused on the removal of the remaining pollutants (CO ,
334 hydrocarbons and soot).

335 Figure 7 shows the conversion percentages and conversion rates of
336 propylene, benzene and CO obtained in steady state at different temperatures.
337 The catalytic activities for the conversion of these three pollutants of the $\text{Ce}_{0.73-x}$
338 $\text{Zr}_{0.27}\text{Nd}_x\text{O}_2$ mixed oxides with $x \leq 0.09$ were significantly higher than those of
339 the mixed oxides with higher neodymium content. This behavior is consistent
340 with the drastic decrease of the BET surface area and surface reducibility of
341 $\text{Ce}_{0.53}\text{Zr}_{0.27}\text{Nd}_{0.2}\text{O}_2$ and $\text{Ce}_{0.43}\text{Zr}_{0.27}\text{Nd}_{0.3}\text{O}_2$ with regard to the $\text{Ce}_{0.73-x}\text{Zr}_{0.27}\text{Nd}_x\text{O}_2$
342 mixed oxides with $x \leq 0.09$.

343 CO conversion started above $300\text{ }^\circ\text{C}$ for all catalysts and increased
344 smoothly with temperature achieving 30 % conversion at $550\text{ }^\circ\text{C}$ for $\text{Ce}_{0.73-x}$

345 $x\text{Zr}_{0.27}\text{Nd}_x\text{O}_2$ mixed oxides with $x \leq 0.09$. Propylene and benzene conversions
346 needed temperatures above 350 and 400 °C, respectively, to occur in
347 measurable extents in the experiment performed with $\text{Ce}_{0.73}\text{Zr}_{0.27}\text{O}_2$, which is
348 the most active catalyst at low temperature among those prepared in this study.
349 The onset temperatures for propylene and benzene conversion were slightly
350 higher for the $\text{Ce}_{0.73-x}\text{Zr}_{0.27}\text{Nd}_x\text{O}_2$ mixed oxides with $x = 0.01, 0.05$ and 0.09 than
351 for $\text{Ce}_{0.73}\text{Zr}_{0.27}\text{O}_2$. However, the conversions rose faster with temperature for
352 these neodymium-containing mixed oxides and they were more active than
353 $\text{Ce}_{0.73}\text{Zr}_{0.27}\text{O}_2$ at the highest temperatures tested. This change of the reaction
354 order of neodymium-free and neodymium-containing Ce-Zr mixed oxides at
355 different temperatures could be related with the surface reducibility of these
356 oxides, as studied by H_2 -TPR (see Figures 5 and 6). The temperature for
357 maximum signal in the surface reduction peak was the lowest for $\text{Ce}_{0.73}\text{Zr}_{0.27}\text{O}_2$
358 (Figure 6), and the onset temperatures for propylene and benzene conversions
359 were also the lowest for this catalyst (Figures 7a and 7b). The surface reduction
360 peak temperature was slightly higher for the $\text{Ce}_{0.73-x}\text{Zr}_{0.27}\text{Nd}_x\text{O}_2$ mixed oxides
361 with $x = 0.01, 0.05$ and 0.09 than for $\text{Ce}_{0.73}\text{Zr}_{0.27}\text{O}_2$ (Figure 6), and so does the
362 onset propylene and benzene conversion temperatures (Figures 7a and 7b,
363 respectively), but once the temperature was high enough for these reactions to
364 occur the conversions rose faster for the neodymium-containing catalysts. This
365 could be tentatively attributed to the improved oxygen mobility upon neodymium
366 doping, which would restore faster the oxygen balance on the catalyst surface
367 after consumption in propylene and benzene oxidation. This agreement
368 between the surface reduction behavior observed by H_2 -TPR experiments and
369 the catalytic combustion of propylene and benzene suggest that redox

370 mechanisms are taking place, as typically occurs in oxidation reactions
371 catalyzed by cerium-based oxides [3, 38].

372 Soot combustion experiments were also performed at 530 °C under the
373 complex gas mixture with O₂, NO_x, H₂O, CO₂, CO, propylene and benzene that
374 simulates a Diesel exhaust, and the soot conversion profiles were plotted in
375 Figure 8 as a function of time. The most active soot combustion Ce_{0.73-}
376 _xZr_{0.27}Nd_xO₂ catalysts are those with x = 0.01, 0.05 and 0.09. These low
377 neodymium atomic fractions improved the Ce_{0.73}Zr_{0.27}O₂ catalytic activity, while
378 the improvement in activity for soot combustion is null for the mixed oxides with
379 higher neodymium atomic fraction (Ce_{0.53}Zr_{0.27}Nd_{0.2}O₂ and Ce_{0.43}Zr_{0.27}Nd_{0.3}O₂).
380 This behavior is in line with the previously discussed conversions of CO,
381 propylene and benzene obtained in experiments performed without soot (Figure
382 7). The improved catalytic activity for soot combustion of the Ce-Zr mixed oxide
383 catalyst by 0.09 atomic fraction neodymium doping was already reported [20],
384 but the current study analyzes the effect of neodymium in a wider range of
385 concentrations and in a more complex gas mixture.

386 The removal of propylene, benzene and CO was analyzed during soot
387 combustion, and the conversion profiles were plotted in Figure 9 with regard to
388 soot conversion. The propylene conversion percentage was around 90% for the
389 Ce_{0.73-x}Zr_{0.27}Nd_xO₂ mixed oxides with x ≤ 0.09, while remained much lower for
390 Ce_{0.53}Zr_{0.27}Nd_{0.2}O₂ and Ce_{0.43}Zr_{0.27}Nd_{0.3}O₂. It was observed that the catalyst
391 temperature (the thermocouple was placed inside the reactor facing the
392 catalytic bed) increased few degrees (~3-5 °C) during the exothermal soot
393 combustion, and this leads to think that the local increase of temperature could

394 be higher in local hot spots at the soot-catalyst particles interface. This could
395 explain why propylene conversions obtained in the presence of soot (Figure 9)
396 were slightly higher than those obtained in the absence of soot (Figure 7).

397 The conversions of benzene during soot combustion were lower than
398 those of propylene (Figure 9), in accordance with the behavior in the absence of
399 soot (Figure 7), and the $\text{Ce}_{0.73-x}\text{Zr}_{0.27}\text{Nd}_x\text{O}_2$ mixed oxides with $x \leq 0.09$ were
400 more active than $\text{Ce}_{0.53}\text{Zr}_{0.27}\text{Nd}_{0.2}\text{O}_2$ and $\text{Ce}_{0.43}\text{Zr}_{0.27}\text{Nd}_{0.3}\text{O}_2$, which showed
401 almost null activity.

402 Finally, the CO conversion profiles obtained in catalytic combustion
403 experiments performed with soot (Figure 9c) were very different to those
404 obtained without soot (Figure 7c). Actually, most CO conversion values were
405 negative during soot combustion, that is, CO was actually emitted in
406 experiments with soot instead of being depleted. The $\text{Ce}_{0.73-x}\text{Zr}_{0.27}\text{Nd}_x\text{O}_2$ mixed
407 oxides with $x = 0.01, 0.05$ and 0.09 reached positive CO conversion values,
408 once soot was consumed (see inset in Figure 9c), what means that there is a
409 net production of CO during soot combustion because the catalytic CO
410 oxidation rates seem to be lower than the CO emission rate by soot
411 combustion. It was estimated in a previous study that 75 % of soot was oxidized
412 to CO_2 in a $\text{Ce}_{0.64}\text{Zr}_{0.27}\text{Nd}_{0.09}\text{O}_2$ -catalysed combustion of soot, while the
413 remaining 25% yielded CO. The emission of CO as soot combustion product
414 could be positive if a deNO_x device (by Selective Catalytic Reduction-SRC or
415 NO_x Storage and Reduction-NSR) is going to be located downstream the ceria-
416 DPF, because CO would contribute to NO_x reduction and would save reductant.
417 On the contrary, if the ceria-DPF is the last device in the after-treatment system

418 actions must be taken to avoid CO release, for instance, including into the DPF
419 a transition metal like copper with high CO oxidation capacity.

420 As a summary, the catalytic tests performed in the current study
421 evidenced that some $\text{Ce}_{0.73-x}\text{Zr}_{0.27}\text{Nd}_x\text{O}_2$ catalysts were able to accelerate
422 simultaneously soot, propylene and benzene combustion. As a general trend,
423 the catalytic behavior of $\text{Ce}_{0.73}\text{Zr}_{0.27}\text{O}_2$ was improved by low atomic fraction
424 neodymium doping ($0.01 \leq x \leq 0.09$), while a very negative effect was obtained
425 for higher loading ($x = 0.2$ and 0.3). The $\text{Ce}_{0.73-x}\text{Zr}_{0.27}\text{Nd}_x\text{O}_2$ mixed oxides were
426 also able to accelerate CO oxidation in a certain extent, but there was a net
427 production of CO during soot combustion because the oxidation capacity of
428 these oxides was not high enough to oxidize all CO released as soot
429 combustion product.

430

431 **4.- Conclusions.**

432 $\text{Ce}_{0.73-x}\text{Zr}_{0.27}\text{Nd}_x\text{O}_2$ mixed oxides ($x = 0, 0.01, 0.05, 0.09, 0.2$ and 0.3)
433 were prepared, characterized, and tested for simultaneous CO, propylene,
434 benzene and soot combustion in simulated Diesel exhaust conditions, and the
435 following conclusions can be summarized:

- 436 • The $\text{Ce}_{0.73-x}\text{Zr}_{0.27}\text{Nd}_x\text{O}_2$ mixed oxides consisted of two segregated ceria-
437 rich and zirconium-rich phases with proper neodymium doping for
438 atomic fractions of $x \leq 0.09$. This was a consequence of the preparation
439 method used, where Ce^{3+} , Nd^{3+} and Zr^{4+} cations were precipitated.

440

- 441 • Doping of the Ce-Zr mixed oxides with low neodymium atomic fractions
442 ($x \leq 0.09$) promoted the creation of oxygen vacancies, had a minor
443 effect on the BET specific surface area of the oxides, increased the
444 amount of surface Ce^{4+} reduced and had a positive effect on the
445 catalytic activity. On the contrary, higher neodymium atomic fractions (x
446 = 0.2 and 0.3) had a negative effect on the mixed oxides features
447 because promoted sintering, with a drastic decrease of the BET specific
448 surface area, surface reducibility, and catalytic activity.
- 449
- 450 • The $\text{Ce}_{0.73-x}\text{Zr}_{0.27}\text{Nd}_x\text{O}_2$ catalysts with $x \leq 0.09$ were able to accelerate
451 simultaneously soot, propylene and benzene oxidation. As a general
452 trend, the catalytic behavior of $\text{Ce}_{0.73}\text{Zr}_{0.27}\text{O}_2$ was improved by low
453 atomic fraction neodymium doping ($0.01 \leq x \leq 0.09$), while a very
454 negative effect was obtained for higher loading ($x = 0.2$ and 0.3).
- 455
- 456 • The $\text{Ce}_{0.73-x}\text{Zr}_{0.27}\text{Nd}_x\text{O}_2$ mixed oxides were also able to accelerate CO
457 oxidation in a certain extent, but there was a net production of CO
458 during soot combustion because the oxidation capacity of these oxides
459 was not high enough to oxidize all CO released as soot combustion
460 product.

461

462 **Acknowledgments**

463 The authors thank the financial support of CNPq – National Counsel of
464 Technological and Scientific Development (Brazil), of the Spanish Ministry of
465 Economy and Competitiveness (Project CTQ2012-30703) and of the UE
466 (FEDER funding).

467

Accepted Manuscript

468 **References**

- 469 [1] G. Kim, *Ind. Eng. Chem. Prod. Res. Dev.* 21 (1982) 267-274.
- 470 [2] A. F. Diwell, R.R. Rajaram, H.A. Shaw, T.J. Truex, *Stud. Surf. Sci. Catal.*
471 71 (1991) 139-152.
- 472 [3] A. Trovarelli, C. De Leitenburg, M. Boaro, G. Dolcetti, *G.Catal. Today* 50
473 (1999) 353-367.
- 474 [4] H. S. Gandhi, G. W. Graham, R.W. McCabe, *J. Catal.* 216 (2003) 433-
475 442.
- 476 [5] E. Aneggi, C. de Leitenburg, G. Dolcetti, A. Trovarelli, *Catal. Today* 114
477 (2006) 40-47.
- 478 [6] A.M. Hernández-Giménez, D. Lozano Castelló, A. Bueno-López, *Chem.*
479 *Pap.* 68 (2014) 1154-1168.
- 480 [7] M. Dhakad, T. Mitsuhashi, S. Rayalu, S. Pradip Doggali, J. Bakardjiva,
481 D. Subrt, H. Fino, N. Haneda, Labhsetwar, *Catal. Today* 132 (2008) 188-
482 193.
- 483 [8] M. Machida, Y. Murata, K. Kishikawa, D. Zhang, K. Ikeue, *Chem. Mater.*
484 20 (2008) 4489-4494.
- 485 [9] A. Bueno-López, *Appl. Catal. B* 146 (2014) 1-11.
- 486 [10] J.P.A. Neeft, M. Makkee, J.A. Moulijn, *Fuel Process. Technol.* 47 (1996)
487 1-69.
- 488 [11] B.A.A.L. van Setten, M. Makkee, J.A. Moulijn, *Catal. Rev.* 43 (2001) 489-
489 564.
- 490 [12] M.V. Twigg, *Appl. Catal. B* 70 (2007) 2-15.
- 491 [13] D. Fino, V. Specchia, *Powder Technol.* 180 (2008) 64-73.
- 492 [14] N. Guillén-Hurtado, A. García-García, A. Bueno-López. *J. Catal.* 299
493 (2013) 181-187.
- 494 [15] A. M. Hernández-Giménez, D. Lozano-Castelló, A. Bueno-López. *Appl.*
495 *Catal. B* 148-149 (2014) 406-414.
- 496 [16] R. Flouty, E. Abi-Aad, S. Siffert, A. Aboukais, *Appl. Catal. B* 46 (2003)
497 145-153.
- 498 [17] D. Weng, J. Li, X. Wu, F. Lin, *Catal. Commun.* 9 (2008) 1898-1901.
- 499 [18] M.A. Peralta, V.G. Milt, L.M. Cornaglia, C.A. Querini, *J. Catal.* 242 (2006)
500 118-130.

- 501 [19] K. Tikhomirov, O. Krocher, M. Elsener, A. Wokaun, *Appl. Catal. B* 64
502 (2006) 72–78.
- 503 [20] A. M. Hernández-Giménez, L. P. dos Santos Xavier, A. Bueno-López,
504 *Appl. Catal. A* 462–463 (2013) 100–106.
- 505 [21] I. Atribak, A. Bueno-Lopez, A. Garcia-Garcia, *J. Catal.* 259 (2008) 123–
506 132.
- 507 [22] I. Atribak, A. Bueno-Lopez, A. Garcia-Garcia, *Top. Catal.* 52 (2009)
508 2088–2091.
- 509 [23] F. Zhang, C.-H. Chen, R.D. Robinson, I.P. Herman, S.-W. Chan, *J. Am.*
510 *Ceram. Soc.* 89 (2006) 1028-1036.
- 511 [24] B.A.A.L. van Setten, J.M. Schouten, M. Makkee, J.A. Moulijn, *Appl.*
512 *Catal. B* 28 (2000) 253-257.
- 513 [25] E. Djurado, P. Bouvier, G. J.Lucazeau, *Solid State Chem.* 149 (2000)
514 399-407.
- 515 [26] R.C. Garvie, *J. Phys. Chem.* 82 (1978) 218-224.
- 516 [27] A. Gayen, M. Boaro, C. de Leitenburg, J. Llorca, A. Trovarelli, *J. Catal*
517 270 (2010) 285-298.
- 518 [28] D. J. Kim, *J. Am. Ceram. Soc.* 72 (1989) 1415-1421.
- 519 [29] M. Mogensen in *Catalysis by ceria and related materials*. A. Trovarelli ed.
520 (2002) Imperial College Press, London. Pag. 462.
- 521 [30] N. Guillén-Hurtado, I. Atribak, A. Bueno-López, A. García-García, *J. Mol.*
522 *Catal. A* 323 (2010) 52-58.
- 523 [31] A. Mineshige, T. Taji, Y. Muroi, M. Kobune, S. Fujii, N. Nishi, M. Inaba, Z.
524 Ogumi, *Solid State Ionics* 135 (2000) 481-485.
- 525 [32] L.N. Ikryannikova, A.A. Aksenov, G.L. Markayan, G.P. Muravieva, B.G.
526 Kostyuk, A.N. Kharlanov, E.V. Linina, *Appl. Catal. A* 210 (2001) 225-235.
- 527 [33] J. Kaspar, P. Fornasiero, G. Balducci, R. di Monte, N. Hickey, V. Sergo,
528 *Inorg. Chim. Acta* 349 (2003) 217–226.
- 529 [34] S. Letichevsky, C.A. Tellez, R.R. de Avillez, M.I.P. da Silva, M.A. Fraga,
530 L.G. Appel, *Appl. Catal. B* 58 (2005) 203–210.
- 531 [35] A. Martínez-Arias, M. Fernández-García, V. Ballesteros, L.N. Salamanca,
532 J.C. Conesa, C. Otero, J. Soria, *Langmuir* 15 (1999) 4796–4802.

- 533 [36] Y.H. Zhang, H.X. Zhang, Y.X. Xu, Y.G. Wang, J. Solid State Chem. 177
534 (2004) 3490-3498.
- 535 [37] Y.H. Zhang, H.L. Xu, Y.X. Xu, H.X. Zhang, Y.G. Wang, J. Photochem.
536 Photobiol. A 170 (2005) 279-285.
- 537 [38] A. Trovarelli, Catal. Rev. Sci. Eng. 38 (1996) 439-520.

Accepted Manuscript

538

539 **Figure captions**

540

- 541 **Figure 1.** X-Ray diffractograms of the $\text{Ce}_{0.73-x}\text{Zr}_{0.27}\text{Nd}_x\text{O}_2$ oxides.
- 542 **Figure 2.** Cell parameter of the $\text{Ce}_{0.73-x}\text{Zr}_{0.27}\text{Nd}_x\text{O}_2$ oxides determined from
543 X-Ray diffractograms.
- 544 **Figure 3.** Raman spectra of the $\text{Ce}_{0.73-x}\text{Zr}_{0.27}\text{Nd}_x\text{O}_2$ oxides. (a) General view
545 of the $100\text{-}1600\text{ cm}^{-1}$ range and (b) detail of the F_{2g} ceria peak
546 centered at $460\text{-}465.8\text{ cm}^{-1}$.
- 547 **Figure 4.** BET specific surface area of the $\text{Ce}_{0.73-x}\text{Zr}_{0.27}\text{Nd}_x\text{O}_2$ oxides.
- 548 **Figure 5.** TCD profiles obtained in temperature programmed reductions with
549 H_2 of the $\text{Ce}_{0.73-x}\text{Zr}_{0.27}\text{Nd}_x\text{O}_2$ oxides.
- 550 **Figure 6.** Temperature of the surface and bulk reduction peaks obtained in
551 H_2 -TPR experiments with the $\text{Ce}_{0.73-x}\text{Zr}_{0.27}\text{Nd}_x\text{O}_2$ oxides.
- 552 **Figure 7.** Catalytic tests performed at different temperatures with the $\text{Ce}_{0.73-x}$
553 $\text{Zr}_{0.27}\text{Nd}_x\text{O}_2$ oxides in the absence of soot. (a) Propylene, (b)
554 benzene and (c) CO.
- 555 **Figure 8.** Soot conversion in catalytic tests performed at $530\text{ }^\circ\text{C}$ with the
556 $\text{Ce}_{0.73-x}\text{Zr}_{0.27}\text{Nd}_x\text{O}_2$ oxides mixed in loose contact with soot.
- 557 **Figure 9.** Catalytic tests performed at $530\text{ }^\circ\text{C}$ with the $\text{Ce}_{0.73-x}\text{Zr}_{0.27}\text{Nd}_x\text{O}_2$
558 oxides mixed in loose contact with soot. (a) Propylene, (b)
559 benzene and (c) CO.

Figure 1

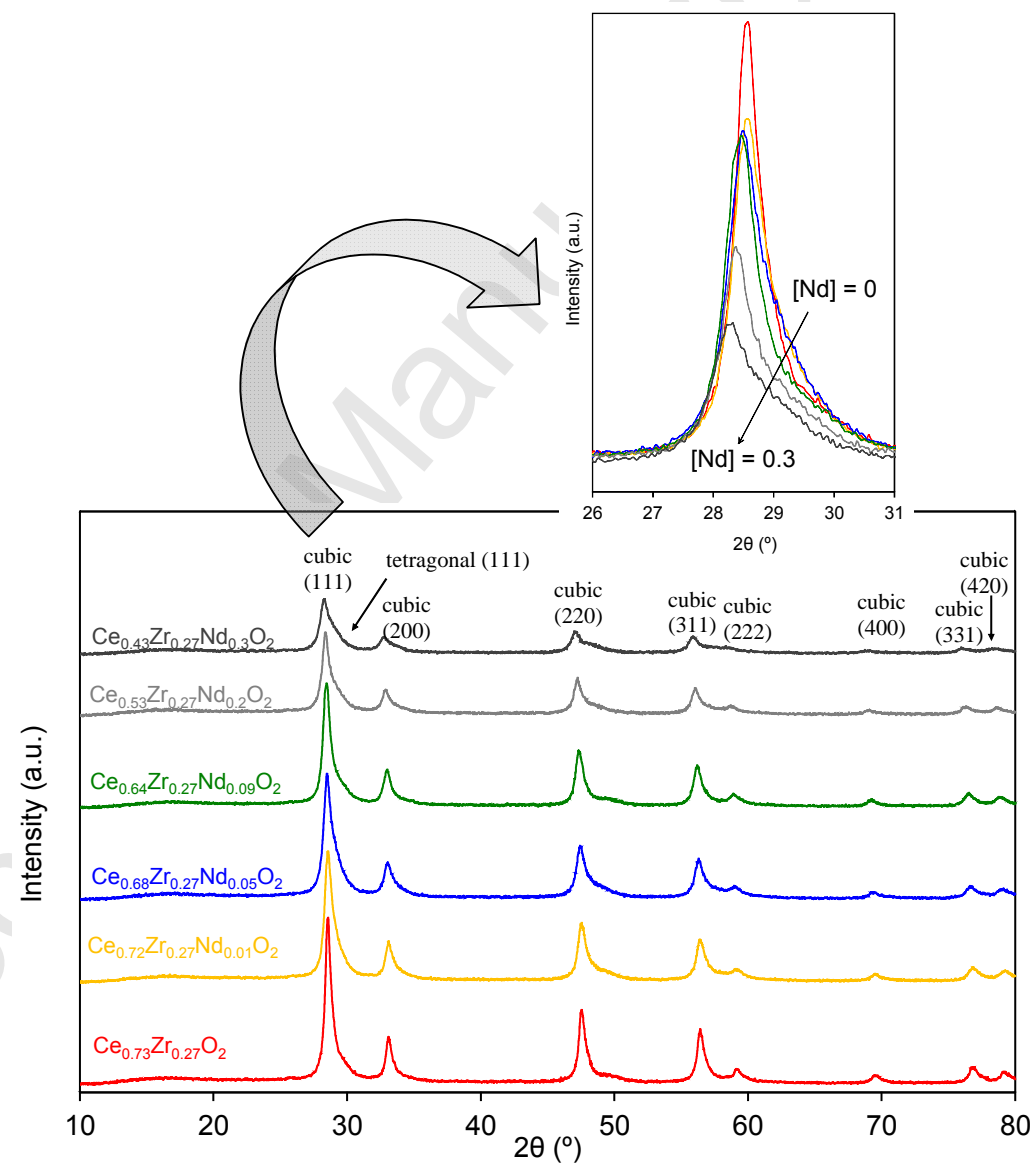


Figure 2

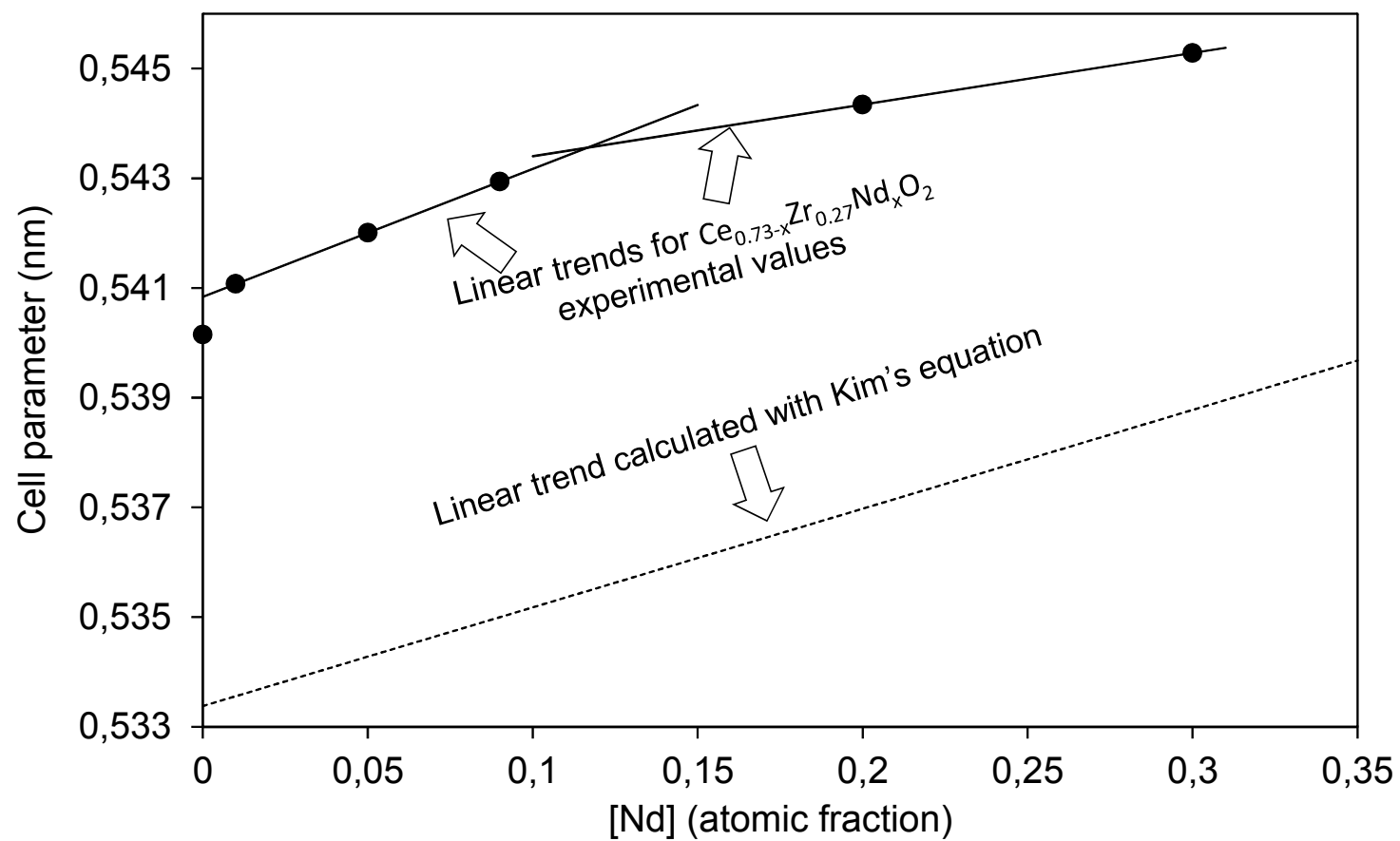


Figure 3

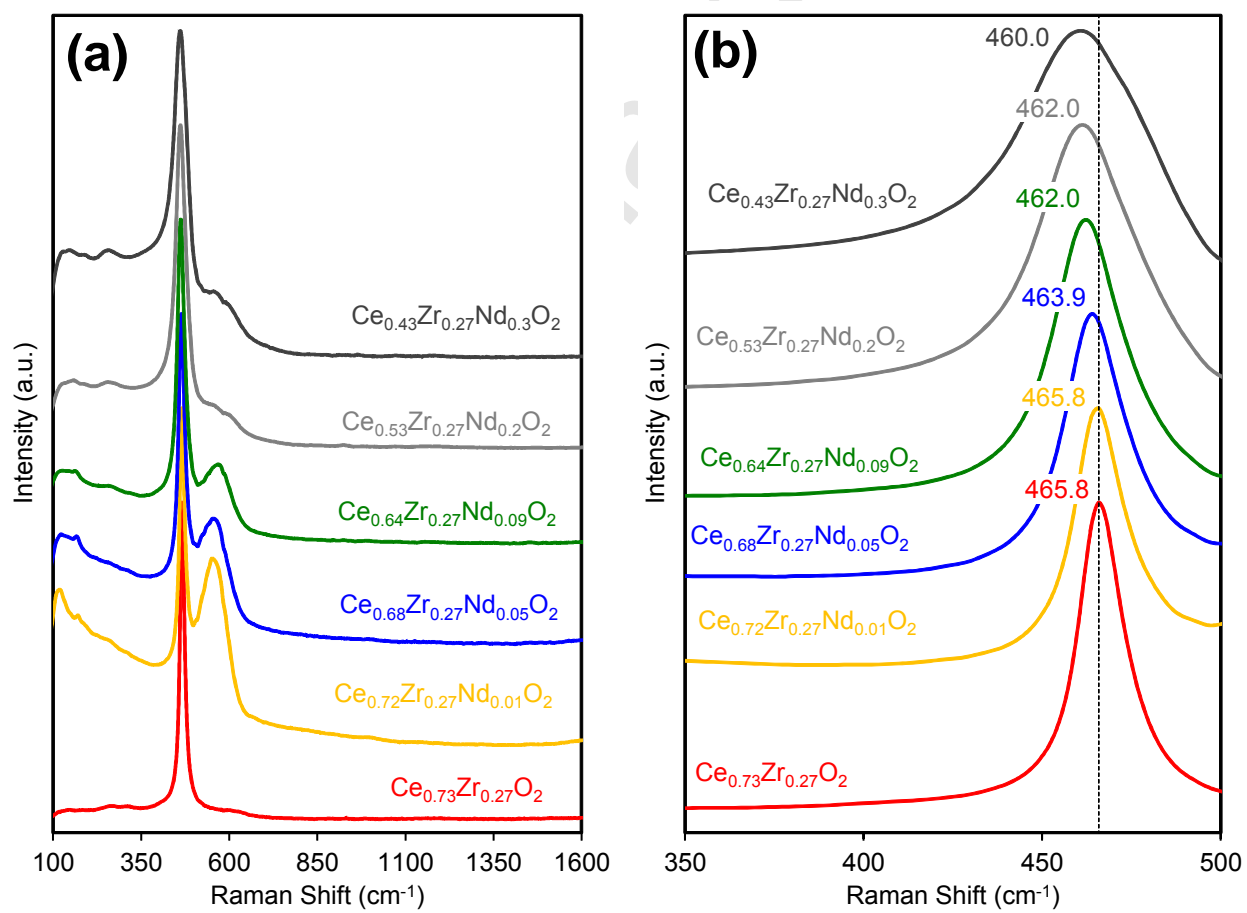
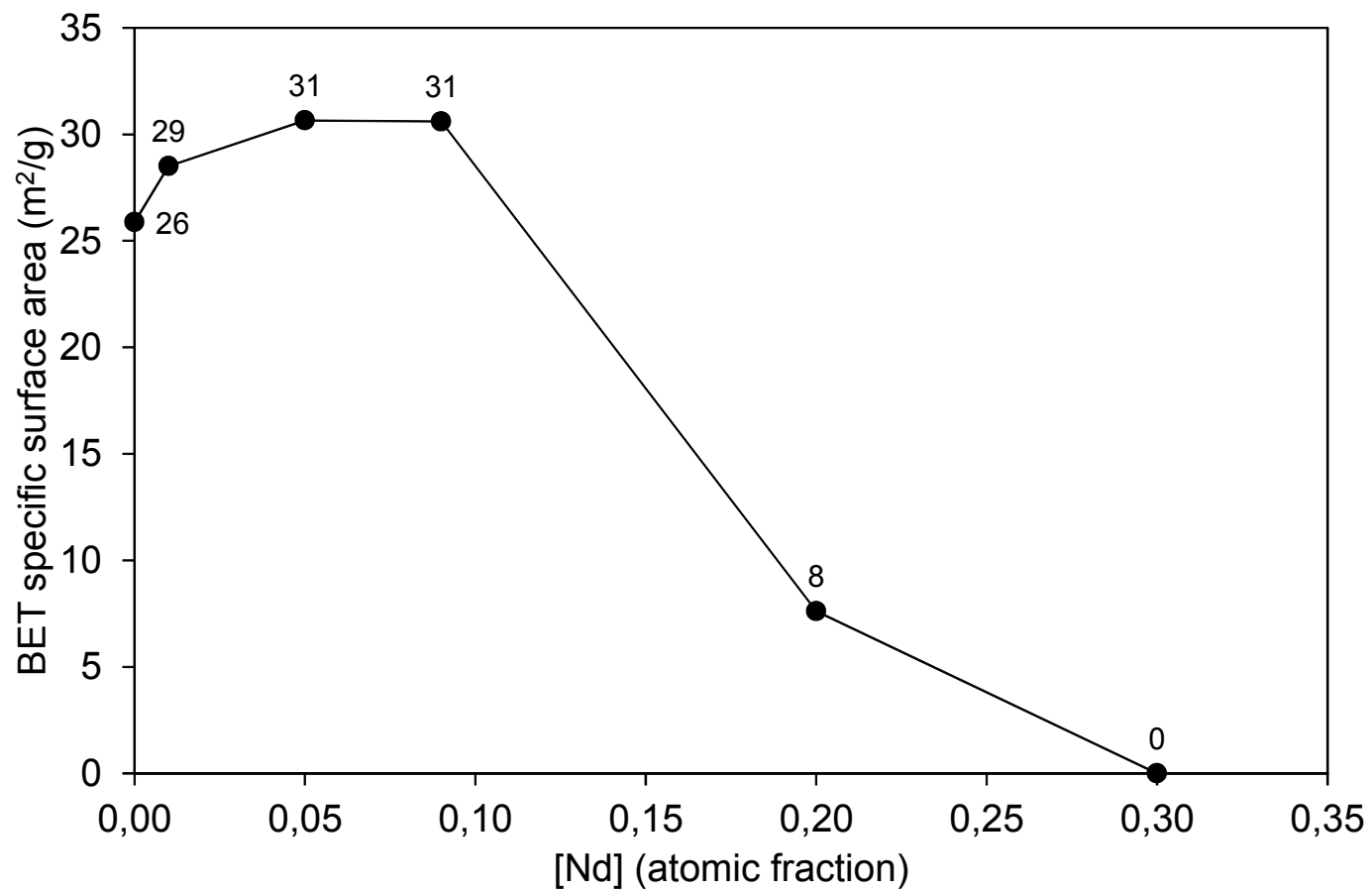


Figure 4



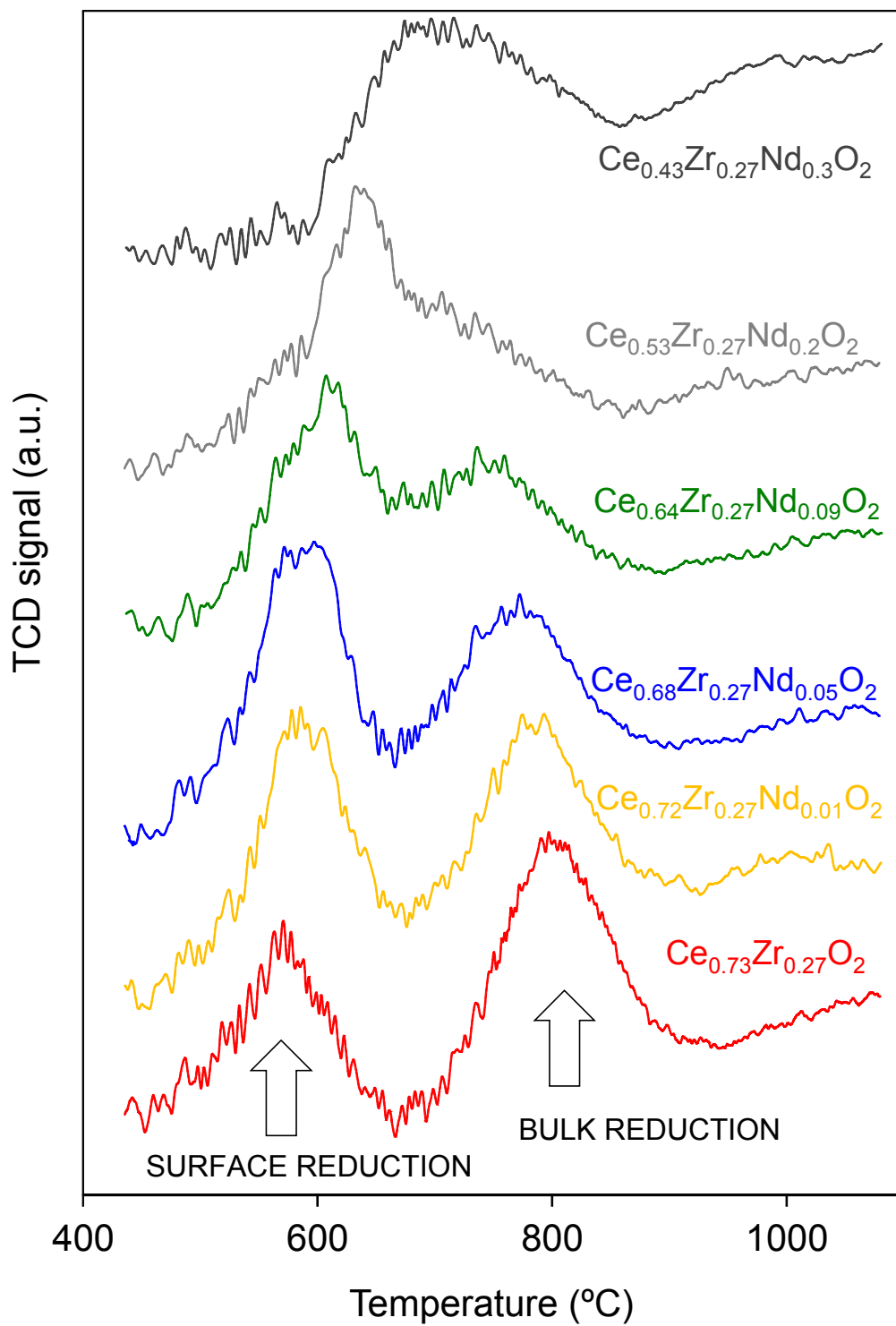
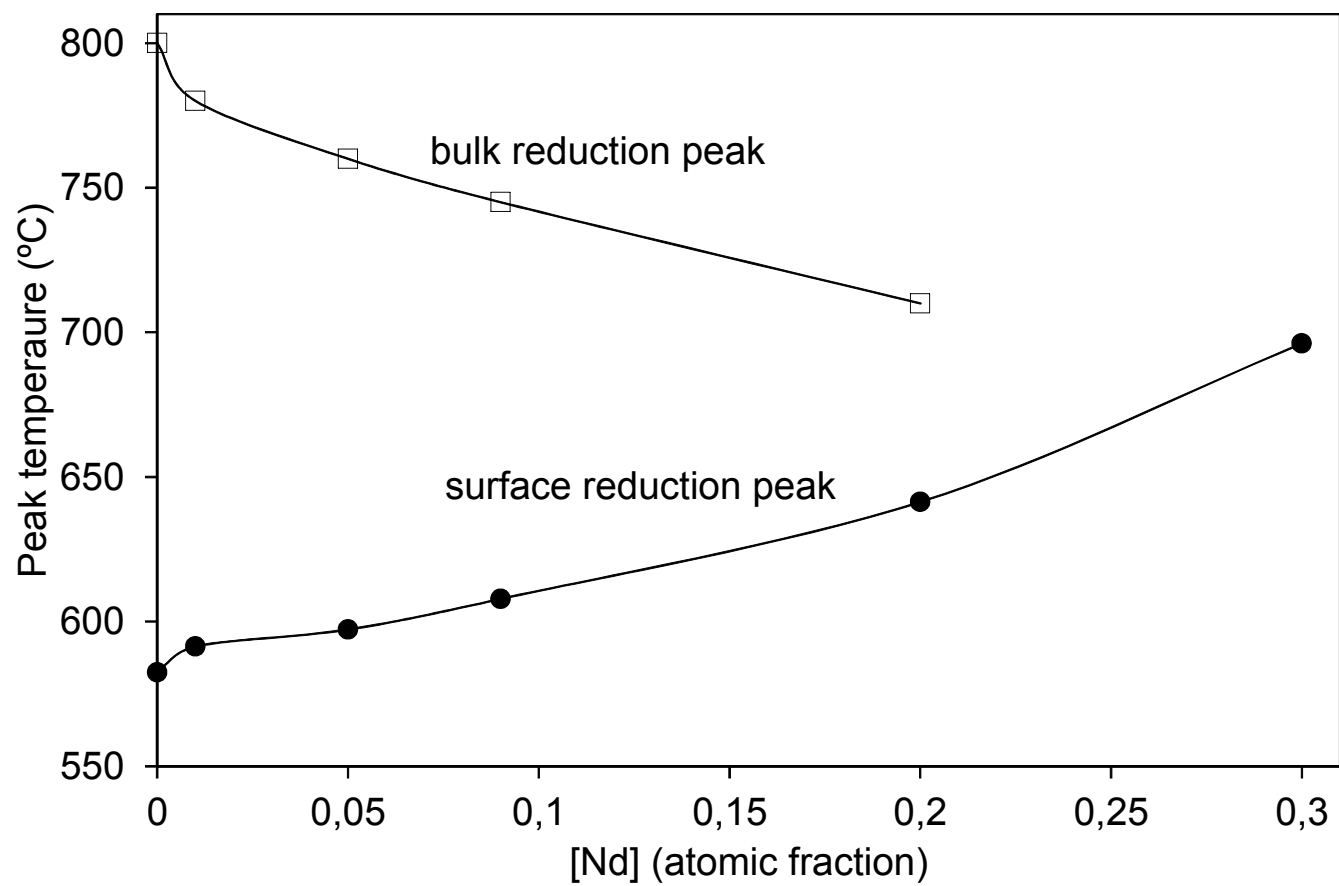
**Figure 5**

Figure 6



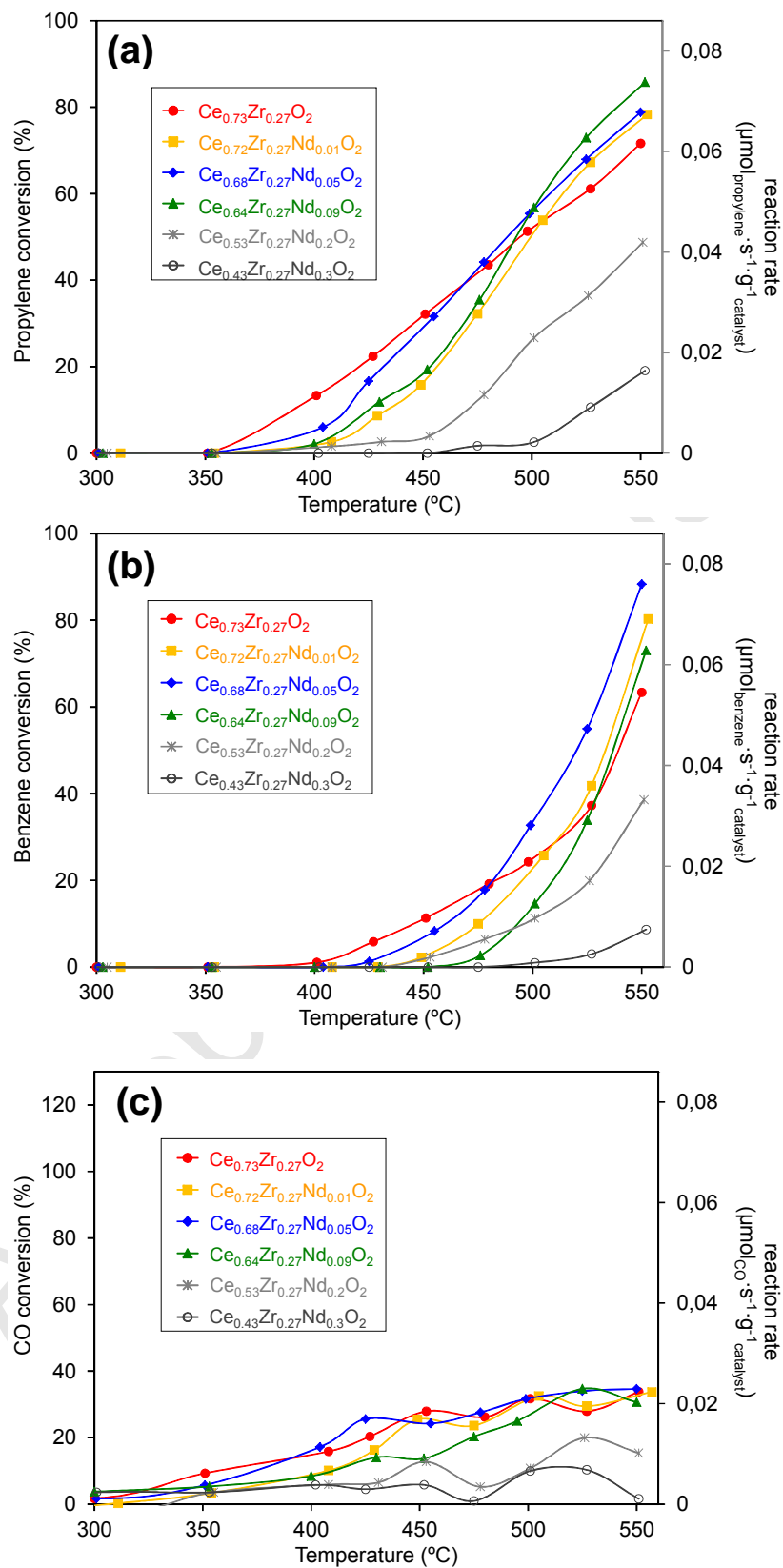
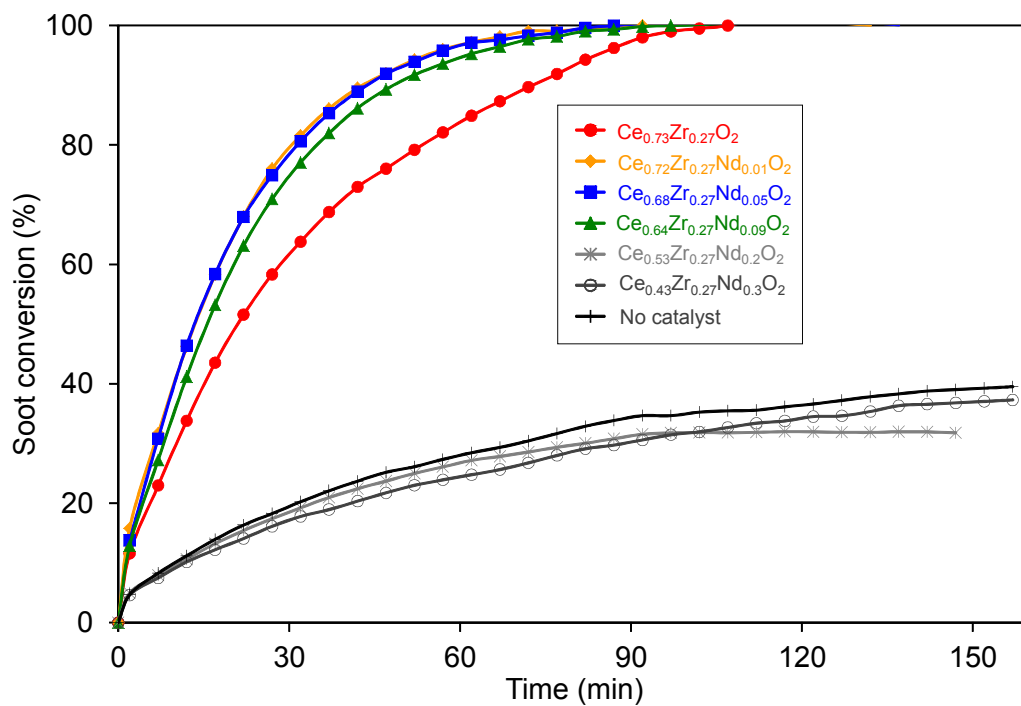


Figure 7

**Figure 8**

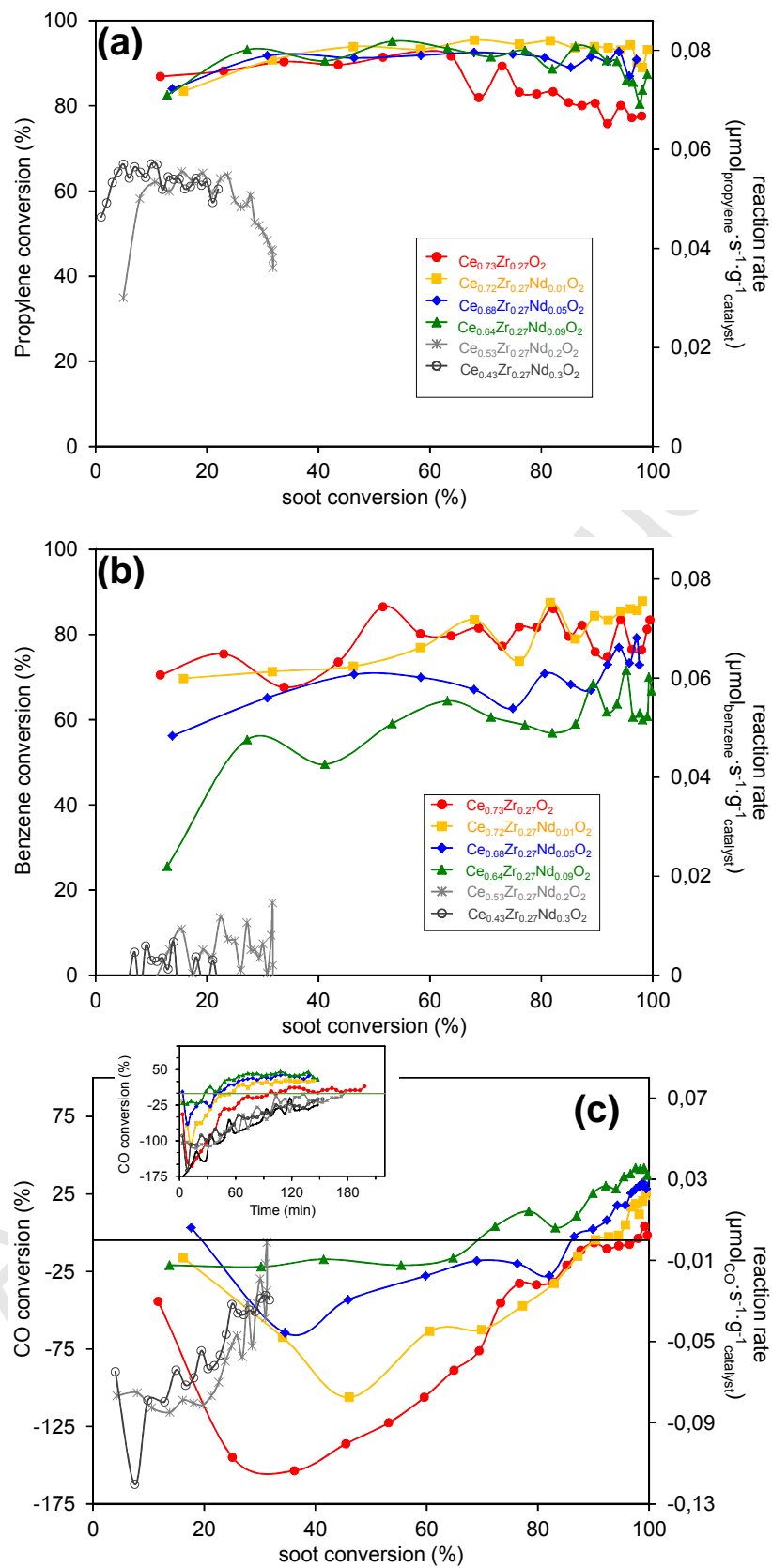
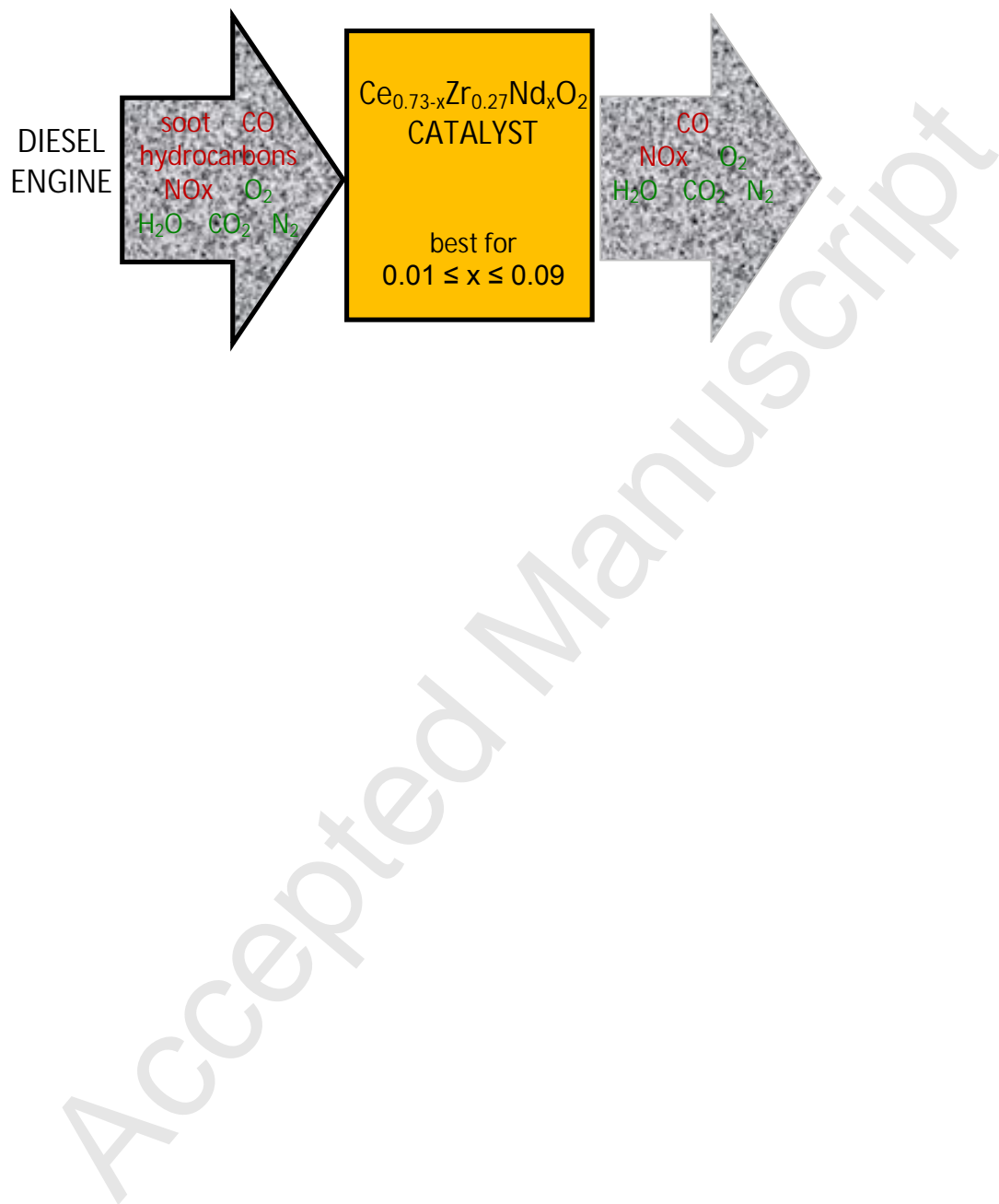


Figure 9

Graphical abstract



Research highlights

- CeZrNd mixed oxides accelerate simultaneously soot, propylene and benzene oxidation
- Best $\text{Ce}_{0.73-x}\text{Zr}_{0.27}\text{Nd}_x\text{O}_2$ catalysts were obtained with $0.01 \leq x \leq 0.09$
- Nd improves surface reducibility and creation of oxygen vacancies